JPE 16-2-32

http://dx.doi.org/10.6113/JPE.2016.16.2.731
ISSN(Print): 1598-2092 / ISSN(Online): 2093-4718

Evaluation and Comparison of the Low-Frequency Oscillation Damping Methods for the Droop-Controlled Inverters in Distributed Generation Systems

Yong Tao*, Yan Deng†, Guangdi Li*, Guipeng Chen*, and Xiangning He*

*,†College of Electrical Engineering, Zhejiang University, Hangzhou, China

Abstract

The droop-based control strategy is widely applied in the interfacing inverters for distributed generation. This can be a problem since low-frequency stability issues may be encountered in droop-based microgrid. The objective of this paper is to classify, evaluate and compare various low-frequency damping methods. First, low-frequency stability problems are analyzed and an equivalent model of a droop-controlled inverter is investigated to classify the damping methods into the source-type damping strategies and the impedance-type damping strategies. Moreover, the lead-lag compensation network insertion control is proposed as a beneficial part of the source-type damping strategies. Then, the advantages and disadvantages of the different types of damping methods are theoretically evaluated and experimentally tested. Furthermore, the damping methods are comprehensively compared to illustrate the application field of each method. Finally, the synthesis of different damping methods to enhance the low-frequency stability is discussed and experimental validation is presented.

Key words: Distributed Generation, Droop Control, Impedance-type Damping Strategy, Low-frequency Stability, Source-type Damping Strategy

I. INTRODUCTION

The application of renewable energy sources and micro-sources keeps growing in recent years [1]. Distributed generation (DG) is a promising form to integrate these resources into the grid. With the development of DG, the concept of microgrid, which contains a number of systematically organized DG units, has been proposed [2]-[5]. In order to provide enhanced reliability and power quality, microgrid should be able to operate in both grid-connected (GC) mode and islanding (IS) mode. Moreover, the droop control method is often applied to avoid circulating currents among the parallel inverters without the use of any critical communication among them [4]-[8].

However, low-frequency oscillation which destabilizes the microgrid and influences the safety of power electronics elements may be introduced with droop-based control [9]-[12]. Low-frequency stability issues are mainly caused by the coupling between active power and reactive power [13], the interaction between the droop loops, and inner voltage and current loops in high droop coefficients [12], [13], and the constant power loads or constant power generators [9], [17]-[21]. In order to solve the stability problems, many active damping methods have been proposed to mitigate the low-frequency oscillation of droop-based microgrid [4], [13]-[16], [22]-[36].

In [22]-[25], power derivative terms are inserted into both the conventional active power-frequency and the reactive power-voltage magnitude droop loops. The low-frequency stability and dynamic performance can be improved with the derivative terms. However, under non-ideal operation conditions, low-frequency noise may be amplified because of the derivative terms if the cut-off frequency of the power calculation low-pass filter (LPF) is not very low. Since dynamic response is sacrificed with a low cut-off frequency,

Manuscript received Jul. 9, 2015; accepted Oct. 8, 2015.
Recommended for publication by Associate Editor Rae-Young Kim.
†Corresponding Author: dengyan@zju.edu.cn
Tel: +86-571-87952416, Fax: +86-571-87951797, Zhejiang University
*College of Electrical Engineering, Zhejiang University, Hangzhou, China

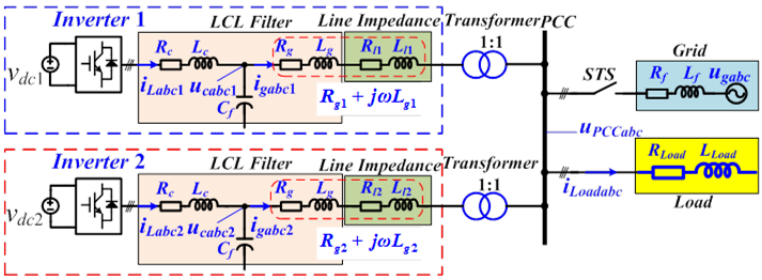

Fig. 1. Structure of the system configuration.

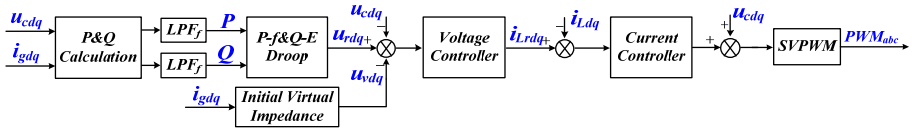

Fig. 2. Block diagram of the conventional control strategy.

the determination of the cut-off frequency needs a tradeoff. The reactive power-voltage magnitude derivative droop is applied in [26] instead of the conventional reactive power-voltage magnitude droop to improve the reactive power sharing among parallel inverters. Moreover, this method can indirectly enhance the low-frequency stability while a complicated restoration mechanism of the voltage magnitude derivative is needed. In order to ensure the low-frequency active damping under different load conditions, the power derivative terms are inserted into the droop loops with adaptive transient droop gains in [27]. Nevertheless, the low-frequency noise problem in [22]-[25] can also be encountered. Moreover, the adaptive droop gains are obtained via small-signal analysis of the power sharing mechanism along the loading trajectory of each DG unit, which significantly increases the computational burden. Furthermore, it is very difficult to guarantee the accuracy of the small-signal analysis. In [28], [29], the feedforward of output current or an increment of active power is inserted into the reference of output voltage. However, the design methods for the feedforward gain and compensation controller are complicated. The feedforward of active power is introduced to accurately link the microgrid frequency dynamics to the motor dynamics in [16] to ensure robust stability under a wide range of droop coefficients. In addition, power system stabilizer (PSS) is an effective method to damp the generator rotor oscillations by controlling the excitation with an auxiliary stabilizing signal, such as speed deviation [30]-[33]. Similarly, low-frequency stability might be improved with the feedforward of the frequency deviation in droop-controlled inverters. In [34], since only the active power droop loop is modified through inserting different compensation networks, the stability improvement is limited. Consequently, the above methods are all implemented by inserting supplementary control loops into the droop loops to enhance the low-frequency stability.

As analyzed in [13]-[15], virtual impedance is a popular method to decouple active power and reactive power, along with improving the low-frequency stability. However, the dynamic response is degraded. In [36], the impacts of inverter output impedance on stability and dynamic performance are investigated, and an inverter current feedforward scheme is proposed to enhance the low-frequency stability. In addition, the output current feedforward scheme can also mitigate the impacts of inverter output impedance on low-frequency stability [11], [37]. However, extra sensors for output current are needed. In conclusion, the low-frequency stability can also be enhanced through changing the low-frequency characteristics of the output impedance.

As mentioned above, many active damping methods have been proposed to solve the low-frequency stability issues in droop-based microgrid. However, there is a lack of systematic evaluation and comparison for different active damping methods. In this paper, the classification, evaluation and comparison for state-of-the-art low-frequency active damping strategies are addressed to give an insightful cognition. The low-frequency stability problems are analyzed and an equivalent model of the droop-controlled inverter is explored to classify the damping methods into the source-type damping strategies and the impedance-type damping strategies. The source-type damping strategies are realized by inserting supplementary control loops into the droop loops, while the impedance-type damping strategies are implemented through changing the low-frequency characteristics of the output impedance. The lead-lag compensation network insertion control is also proposed as a beneficial part of the source-type damping strategies. Then, the advantages and disadvantages of different damping methods are theoretically evaluated and experimentally tested. Moreover, a comprehensive comparison is implemented to illustrate the application field of each method. Finally, the synthesis of different damping strategies to enhance the stability is discussed, and experimental validation is also presented.

The paper is organized as follows. The low-frequency stability of the conventional control strategy and a classification of the existing damping methods are investigated in section II. The source-type damping strategies are introduced in section III. The impedance-type damping strategies are evaluated in section IV. Experimental validation of different damping methods is illustrated in section V. The comparison and synthesis of different damping strategies are discussed in section VI. The last section summarizes the investigation.

II. Low-frequency Stability of the Conventional Control Strategy

In general, voltage source inverter (VSI) is applied as the interface to connect DG units to the grid. A simplified system configuration, as shown in Fig. 1, is used to implement the theoretical analysis. A three-phase VSI with an LCL filter is considered in this paper. L_c is the inverter-side filter inductor and R_c is the equivalent series resistor (ESR). C_f is the filter capacitor. L_g consists of the grid-side inductor of the LCL filter, the leakage inductor of the isolation transformer and the line inductance, and R_g is the ESR. L_f is the feeder inductance and R_f is the ESR. i_{Labc}, u_{cabc}, i_{gabc} and u_{gabc} are the inverter-side current, the voltage of the filter capacitor, the grid-side current (or output current) and the grid voltage in GC mode or the load voltage in IS mode. Since droop-based microgrid can operate in both GC mode and IS mode, the stability analysis in both operation modes needs to be considered. In this paper, one inverter is considered in GC mode to simplify the analysis while two parallel inverters are analyzed in IS mode.

The conventional control strategy for the DG interfacing VSIs is shown in Fig. 2 [5], [36], [38]. As shown, the control strategy consists of active power-frequency and reactive power-voltage magnitude droop loops, initial virtual impedance, and inner voltage and current loops. The detailed explanations of the three parts can be found in [11], [36], [38], which is not introduced here.

In order to further investigate the low-frequency stability of the conventional control strategy, the analysis is implemented. (Note that the low-frequency range is mainly below 10Hz in this paper.) Meanwhile, the classification of the existing low-frequency oscillation damping methods is also given in this section.

A. Low-frequency Stability Issues

The small-signal representation as shown in (1) can be achieved from the droop loops, while (2) can be achieved by combining the inner loops with power calculation [36].

$$\begin{bmatrix}\Delta E\\ \Delta\delta\end{bmatrix}=\begin{bmatrix}k_q & 0\\ 0 & k_p\dfrac{1}{s}\end{bmatrix}\left(\begin{bmatrix}\Delta Q_0\\ \Delta P_0\end{bmatrix}-\begin{bmatrix}\Delta Q\\ \Delta P\end{bmatrix}\right) \tag{1}$$

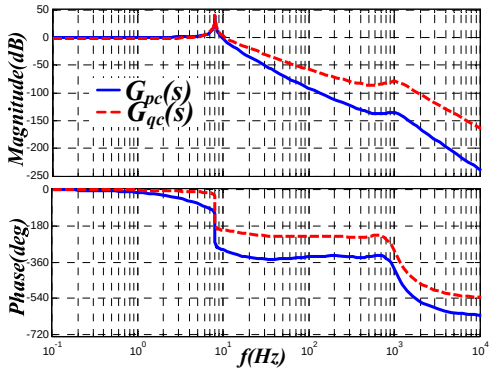

(a)

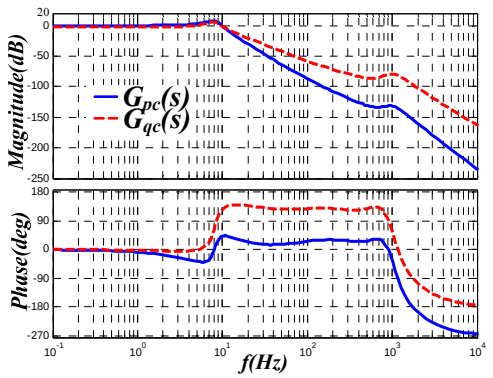

(b)

Fig. 3. Bode diagram of closed-loop transfer function of droop loops for conventional control strategy in GC mode. (a) k_p=0.94×10^{-3}. (b) k_p=1.57×10^{-3}.

$$\begin{bmatrix}\Delta P\\ \Delta Q\end{bmatrix}=\begin{bmatrix}B_1 & B_2E_0\\ B_2 & -B_1E_0\end{bmatrix}\begin{bmatrix}\Delta E\\ \Delta\delta\end{bmatrix} \tag{2}$$

where Δ denotes the perturbed value, δ and E are the phase and amplitude of the output voltage reference, E_0 is the nominal amplitude, P and Q are the active and reactive power, P_0 and Q_0 are their references, and k_p and k_q are the droop coefficients, respectively. In addition, the derivation of B_1 and B_2 can be found in [36], which is not introduced in this paper.

Substituting (1) into (2), (3) can be obtained.

$$\begin{bmatrix}\Delta P\\ \Delta Q\end{bmatrix}=\begin{bmatrix}k_p\dfrac{1}{s}B_2E_0 & k_qB_1\\ -k_p\dfrac{1}{s}B_1E_0 & k_qB_2\end{bmatrix}\left(\begin{bmatrix}\Delta P_0\\ \Delta Q_0\end{bmatrix}-\begin{bmatrix}\Delta P\\ \Delta Q\end{bmatrix}\right) \tag{3}$$

Finally, closed-loop transfer functions of the active power-frequency and reactive power-voltage magnitude droop loops in GC mode can be manipulated as (4) and (5), respectively.

$$G_{pc}(s)=\frac{\Delta P}{\Delta P_0}\Big|_{\Delta Q_0=0}=\frac{k_pB_2E_0+k_pk_qE_0(B_2^2+B_1^2)}{(1+k_qB_2)s+k_pB_2E_0+k_pk_qE_0(B_2^2+B_1^2)} \tag{4}$$

$$G_{qc}(s)=\frac{\Delta Q}{\Delta Q_0}\Big|_{\Delta P_0=0}=\frac{k_qB_2s+k_pk_qE_0(B_2^2+B_1^2)}{(1+k_qB_2)s+k_pB_2E_0+k_pk_qE_0(B_2^2+B_1^2)} \tag{5}$$

TABLE I
POWER STAGE PARAMETERS

Parameter	Symbol	Value
DC Voltage	v_{dc1}, v_{dc2}	$600V$
Grid Frequency	ω_0	$2\pi\cdot50rad/s$
Grid Voltage (Line-Line RMS)	E_0	$346V$
Inverter-side Filter Inductor	L_c, R_c	$8mH$, 0.3Ω
Filter Capacitor	C_f	$4.7\mu F$
Grid-side Inductor	L_g, R_g	$10mH$, 2.4Ω
Feeder Impedance	L_f, R_f	$0.2mH$, 0.2Ω
Switching Frequency	f_s	$10kHz$

TABLE II
CONTROL PARAMETERS

Parameter	Symbol	Value
Droop Coefficients	k_p	$1.57\times10^{-3}rad/(W\cdot s)$
	k_q	$0.0346V/Var$
Cut-off Frequency of Power Calculation LPF_f	ω_f	$2\pi\cdot10rad/s$
Voltage Loop PI	k_{pv}, k_{iv}	0.015, 10
Initial Virtual Impedance	R_{v0}, L_{v0}	0.2Ω, $3mH$
Current Loop PI	k_{pi}, k_{ii}	70, 400

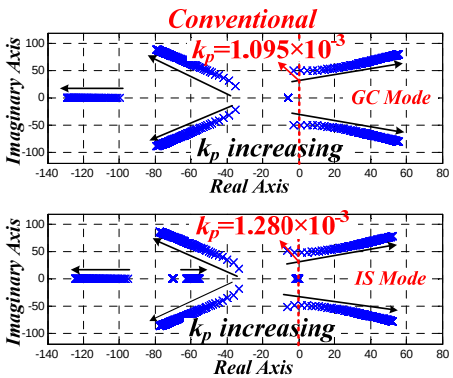

Fig. 4. Root locus diagram of the low-frequency dominant eigenvalues for $0.785\times10^{-3}\le k_p\le31.4\times10^{-3}$ in different operation modes.

Bode diagram of both $G_{pc}(s)$ and $G_{qc}(s)$ is given in Fig. 3 with the parameters listed in Table I and Table II. As shown in Fig. 3(a), low-frequency resonance peak appears in both $G_{pc}(s)$ and $G_{qc}(s)$, even with a small active power droop coefficient k_p, which can induce instability. Instability occurs if k_p is increased to the rated value as presented in Fig. 3(b), and the phase lead happens in the presence of right-half plane poles, which can be verified through Fig. 4.

Low-frequency dominant eigenvalues in GC mode can be obtained by calculating the poles of the closed-loop transfer functions of the droop loops. In IS mode, the state variables can be defined as (6):

$$\boldsymbol{X}_{inv}=\begin{bmatrix}\delta & P & Q & \phi_{dq} & \gamma_{dq} & i_{Ldq} & u_{cdq} & i_{gdq}\end{bmatrix}^T \tag{6}$$

where i^*_{Ldq} is the reference of the inner current loop and:

$$\begin{aligned}\frac{d\phi_{dq}}{dt}&=u_{rdq}-u_{vdq}-u_{cdq}\\ \frac{d\gamma_{dq}}{dt}&=i^*_{Ldq}-i_{Ldq}\end{aligned} \tag{7}$$

Following the modeling approach in [11], the complete system model can be obtained:

$$\begin{bmatrix}\Delta\dot{\boldsymbol{X}}_{inv1}\\ \Delta\dot{\boldsymbol{X}}_{inv2}\\ \Delta\dot{i}_{LoadDQ}\end{bmatrix}=\boldsymbol{A}_{sys}\begin{bmatrix}\Delta\boldsymbol{X}_{inv1}\\ \Delta\boldsymbol{X}_{inv2}\\ \Delta i_{LoadDQ}\end{bmatrix} \tag{8}$$

where Δi_{LoadDQ} denotes the small-signal perturbation of the load current in the common reference frame, $\Delta\boldsymbol{X}_{inv1}$ and $\Delta\boldsymbol{X}_{inv2}$ are small-signal perturbations of the state variables for inverter 1 and inverter 2. The stability in IS mode can be judged through analyzing the low-frequency eigenvalues of $\boldsymbol{A}_{sys}$. Therefore, low-frequency dominant eigenvalues in different operation modes can be acquired as presented in Fig. 4. As shown, stability margin of the conventional control strategy is very low since the dominant low-frequency eigenvalues are very close to the imaginary axis. (Note that stability is mainly influenced by the value of k_p in droop-controlled inverters [11], and stability margin is specially defined as the difference between the value of k_p at the critical stable state and the rated value in this paper.) Moreover, the system becomes unstable with a small droop coefficient k_p, which significantly limits the adjustment range of energy management in autonomous microgrid [12], [36].

B. Classification of Low-frequency Oscillation Damping Methods

In order to mitigate the low-frequency resonance and improve the stability, many oscillation damping methods have been proposed [4], [13]-[16], [22]-[36]. In this paper, the classification of the existing damping methods is implemented according to the equivalent model of the droop-controlled VSI in [36], [38]. From [36] and [38], (9) can be derived.

$$u_{cdq}=G_{clu}(s)u_{rdq}-\boldsymbol{Z}_{ov}(s)i_{gdq} \tag{9}$$

where $G_{clu}(s)$ is the closed-loop transfer function of the voltage loop, $\boldsymbol{Z}_{ov}(s)$ is the equivalent output impedance matrix, u_{cdq} and i_{gdq} are the filter capacitor voltage and grid-side current in synchronous rotating frame (SRF), and u_{rdq} is the reference for the voltage loop which is shown in Fig. 2.

From (9), it can be seen that the output voltage u_{cdq} is mainly determined by the controlled voltage source $G_{clu}(s)u_{rdq}$ and the output impedance $Z_{ov}(s)$. Thus, low-frequency oscillation damping can be carried out by changing the low-frequency characteristics of the controlled voltage source and the output impedance. Since the control bandwidth of $G_{clu}(s)$ is determined by the switching frequency and the control bandwidth of the inner current loop, the

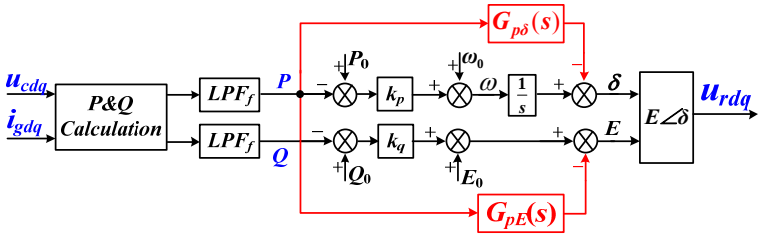

Fig. 5. Block diagram of the APFC scheme.

low-frequency function of the controlled voltage source is dominated by u_{rdq}, which is decided by the droop loops. Consequently, the existing low-frequency oscillation damping methods can be classified into two categories, i.e., the source-type damping strategy and the impedance-type damping strategy. The source-type damping strategy is mainly implemented through inserting supplementary control loops into the droop loops, while the impedance-type damping strategy is mainly realized by introducing current feedforward to alter the low-frequency characteristic of the output impedance. Although both methods can enhance the low-frequency stability, their detailed impacts on the inverter performance are different. Therefore, the analysis, evaluation and comparison of different low-frequency active damping methods are discussed in this paper to better illustrate the diversity of performance impacts. In order to establish a fair comparison among the different active damping methods, the design for the control parameters of the damping methods is based on a common target which is to reduce the values of the resonant peak in $G_{pc}(s)$ and $G_{qc}(s)$ to be both lower than 5dB.

III. Evaluation of the Source-type Damping Strategies

As mentioned in section II, the source-type active damping methods are implemented with supplementary control loops to change the voltage reference u_{rdq}. As seen in [4], [16], [22]-[33], there are two kinds of implementations. The one is to introduce the feedforward of active power, the increment of angular frequency, or the increment of active power. The other is to insert compensation networks into the droop loops and introduce the feedforward of output current. The closed-loop transfer functions of the source-type damping methods can be achieved with the same derivation method in section II-A by modifying (1) according to the corresponding structure of the droop loops. The detailed investigation is given as follows.

A. Active Power Feedforward Control (APFC)

The feedforward item can be active power [16], the increment of active power [29], or the increment of angular frequency [30]-[33]. All the feedforward methods listed above can be equivalent to the feedforward of active power, but with different feedforward compensation networks $G_{p\delta}(s)$ and $G_{pE}(s)$, as shown in Fig. 5. In this paper, $G_{p\delta}(s)$ and $G_{pE}(s)$ are given as:

$$G_{p\delta}(s)=0,\ G_{pE}(s)=\frac{k_1 s}{\tau s+1}\cdot\frac{1+s/T_1}{1+s/T_2} \tag{10}$$

where k_1=5×10^{-2}, τ=1/(2π·50), T_1=2π·15 and T_2=2π·0.5. The design of the parameters is from reference [29].

Similarly, the closed-loop characteristics of the droop loops and the root locus of the low-frequency dominant eigenvalues are shown in Fig. 6. As seen in Fig. 6(a), the resonance peak is effectively mitigated with the APFC scheme. Meanwhile, the stability margin is obviously enhanced in both GC and IS mode through comparing Fig. 6(b) with Fig. 4. However, the feedforward compensation networks need to be carefully designed since stability is very sensitive to the parameters and structure of the compensation

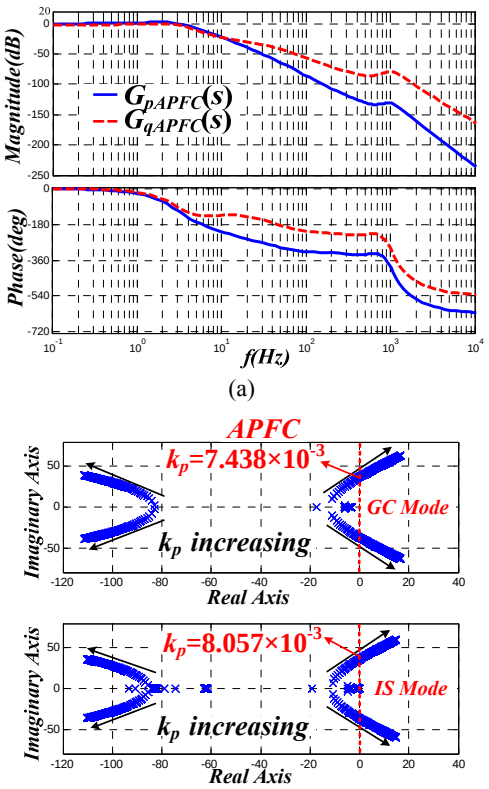

Fig. 6. APFC scheme. (a) Closed-loop characteristics of droop loops in GC mode. (b) Root locus of low-frequency dominant eigenvalues for 0.785×10^{-3}≤k_p≤31.4×10^{-3} in different operation modes.

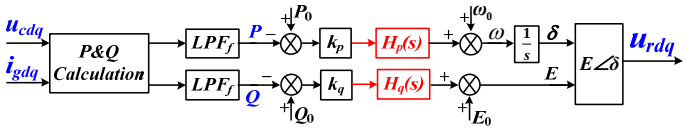

Fig. 7. Block diagram of the CNIC scheme.

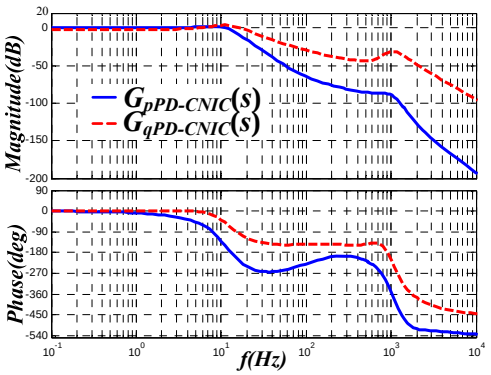

(a)

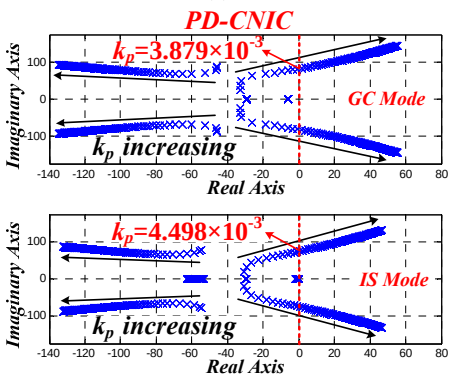

(b)

Fig. 8. PD-CNIC scheme. (a) Closed-loop characteristics of droop loops in GC mode. (b) Root locus of low-frequency dominant eigenvalues for $0.785\times10^{-3}\leq k_p\leq31.4\times10^{-3}$ in different operation modes.

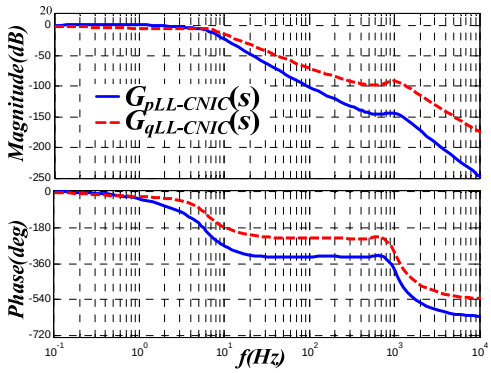

(a)

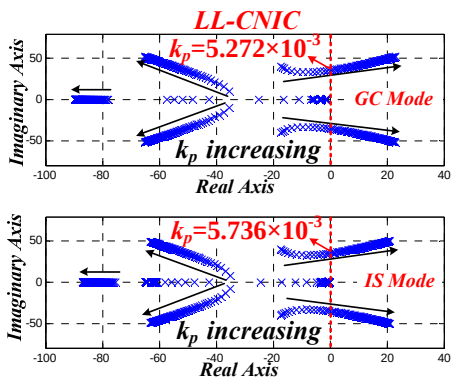

(b)

Fig. 9. Proposed LL-CNIC scheme. (a) Closed-loop characteristics of droop loops in GC mode. (b) Root locus of low-frequency dominant eigenvalues for $0.785\times10^{-3}\leq k_p\leq31.4\times10^{-3}$ in different operation modes.

networks. Moreover, the coupling between active power and reactive power may be strengthened for introducing the active power into the reactive power droop loop.

B. Compensation Network Insertion Control (CNIC)

The compensation network insertion control scheme is presented in Fig. 7. Typically, the compensation networks $H_p(s)$ and $H_q(s)$ are proportional terms [4]. Nevertheless, proportional-derivative (PD) compensation networks [22]-[27] are beneficial for improving stability. In addition, lead-lag (LL) compensation networks are proposed in this paper to enhance the stability. Actually, the feedforward of output current to enhance stability in [28] can also be classified as a CNIC scheme. Two typical compensation network insertion control schemes are evaluated below.

1) Proportional-derivative Compensation Network Insertion Control (PD-CNIC): The PD compensation networks are shown as (11):

$$H_p(s)=1+k_{pd}s,\quad H_q(s)=1+k_{qd}s \tag{11}$$

where $k_{pd}=2\times10^{-3}$ and $k_{qd}=4\times10^{-2}$. The design process of the control parameters can be seen in [24].

As shown in Fig. 8(a), the resonance peak can be suppressed with the PD-CNIC scheme. Moreover, the control bandwidth of the droop loops is increased. Therefore, the interaction with the inner loops in high droop coefficients may deteriorate the stability. As seen in Fig. 8(b), the value of k_p in the stability boundary is only 2.5 times larger than that in the conventional control strategy and the stability margin is worse than the APFC scheme. Therefore, the stability margin and the adjustment range are still limited with the PD-CNIC scheme since there is only one degree of freedom in the PD compensation networks. Meanwhile, low-frequency noise might be introduced with the derivative terms under non-ideal operation conditions. Although low-frequency noise can be suppressed by reducing the cut-off frequency of the power calculation LPF_f, the dynamic response would be degraded. Consequently, a tradeoff needs to be considered when designing the cut-off frequency with the PD-CNIC scheme.

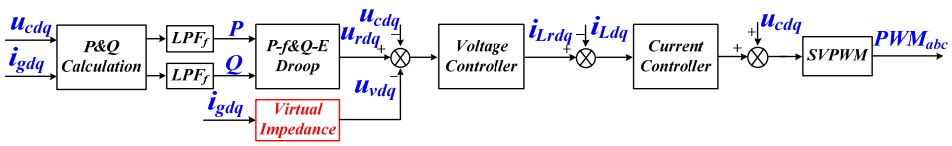

Fig. 10. Block diagram of the VIC scheme.

2) Proposed Lead-lag Compensation Network Insertion Control (LL-CNIC): As illustrated by the PD-CNIC scheme, one-order proportional-derivative controllers are effective for realizing active damping. However, low-frequency noise may be induced by the derivative terms under non-ideal conditions.

In addition, the frequency of the low-frequency oscillation in the unstable state is often close to the cut-off frequency of the power calculation LPF. Therefore, an additional LPF structure can be combined with the proportional-derivative controller to filter out the low-frequency noise and the low-frequency oscillation. Moreover, the cut-off frequency of the LPF should be lower than that of the power calculation LPF. Essentially, the combination of a LPF and a proportional-derivative controller forms a lead-lag controller. Consequently, the lead-lag controller is effective for improving the stability. One-order LL compensation networks are adopted in this paper to illustrate the impacts of the LL-CNIC scheme and the compensation networks are given as (12).

$$H_p(s)=\frac{1+s/T_{p1}}{1+s/T_{p2}},\quad H_q(s)=\frac{1+s/T_{q1}}{1+s/T_{q2}} \tag{12}$$

where T_{p1}=1.257, T_{p2}=0.314, T_{q1}=5.027 and T_{q2}=1.257. The design is based on the closed-loop characteristics and the low-frequency root-locus as shown in Fig. 9.

Compared with the PD-CNIC scheme, there are two degrees of freedom in the LL compensation networks with the LL-CNIC scheme. Therefore, the adjustment of stability margin is more flexible than PD-CNIC scheme. As shown in Fig. 9, the resonance peak can be effectively suppressed and the stability margin is also improved compared with the PD-CNIC scheme. In addition, high order LL compensation networks can also be applied to realize more control degrees of freedom. Meanwhile, the adjustment range of the stability and dynamic performance is also expanded with high order LL compensation networks. Therefore, the proposed LL-CNIC scheme can be a good choice to improve the stability.

IV. Evaluation of the Impedance-type Damping Strategies

According to (9), low-frequency stability is also influenced by the output impedance. Therefore, low-frequency oscillation damping methods can be realized by changing the output impedance characteristics. Moreover, these implementations are divided into two types in this paper. The first type is to insert virtual impedance [13]-[15]. The second type is to introduce output current or inverter current feedforward to mitigate the impacts of inverter output impedance [36], [37]. The closed-loop transfer functions of the impedance-type damping methods can be achieved with the derivation method discussed in section II-A through modifying B_1 and B_2 in (2) according to the corresponding structure of the current feed-forward control. The detailed analysis is given as below.

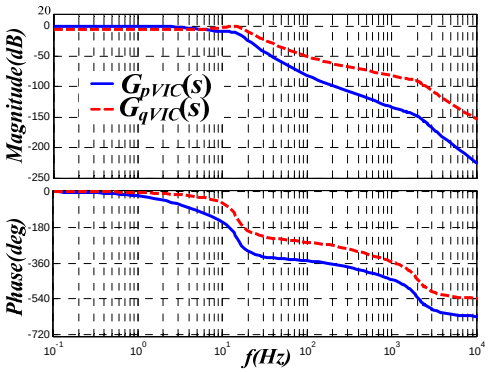

(a)

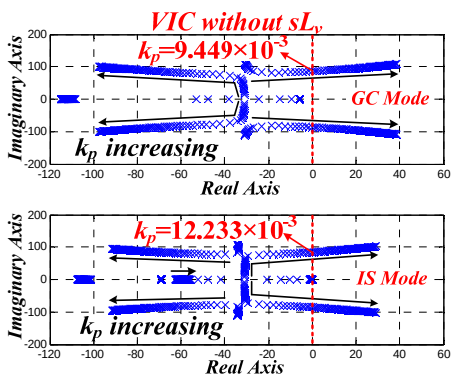

(b)

Fig. 11 VIC scheme. (a) Closed-loop characteristics of droop loops in GC mode. (b) Root locus of low-frequency dominant eigenvalues for $0.785\times10^{-3}\le k_p\le31.4\times10^{-3}$ in different operation modes without sL_v.

A. Virtual Impedance Control (VIC)

The original purpose of virtual impedance is to decouple the active power and the reactive power [4], [5], [13]-[15]. Nevertheless, active damping is also reinforced along with introducing virtual impedance. The VIC scheme is implemented by introducing the feedforward of the grid-side current as presented in Fig. 10. The difference between Fig.

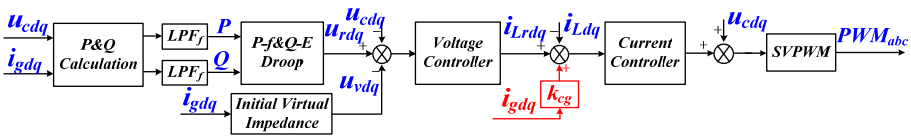

Fig. 12. Block diagram of the OCFC scheme.

10 and Fig. 2 is the larger value of the virtual impedance for the VIC scheme, which means better damping. The voltage drops across the virtual impedance in SRF shown in Fig. 10 can be expressed as (13):

$$\begin{bmatrix} u_{vd} \\ u_{vq} \end{bmatrix} = \begin{bmatrix} R_v + sL_v & -\omega L_v \\ \omega L_v & R_v + sL_v \end{bmatrix} \begin{bmatrix} i_{gd} \\ i_{gq} \end{bmatrix} \tag{13}$$

where R_v and L_v are the virtual resistance and inductance, and ω is the angular frequency of the inverter. In this paper, R_v and L_v are set to 2Ω and 30mH for the VIC scheme. The design process of the virtual impedance is described in reference [13].

As shown in Fig. 11, the resonance peak is mitigated and the stability is enhanced through introducing virtual impedance. Nevertheless, the control bandwidth is reduced and the dynamic response is degraded. In addition, the harmonic performance and voltage unbalance compensation are also influenced by the virtual impedance [38], [39]. Therefore, a tradeoff needs to be made when designing the virtual impedance. Since high-frequency noise might be introduced with the derivative term sL_v, sL_v is often ignored in practical applications.

B. Mitigation of Inverter Output Impedance Impacts (MIOII)

As analyzed in [36], the inverter output impedance with the conventional control strategy can be expressed as (14):

$$Z_o(s) = \frac{\frac{1}{sC_f}}{1 + \frac{1}{sC_f} G_{uc}(s) G_{cli}(s)} \tag{14}$$

where $G_{uc}(s)$ is the PI controller for the voltage loop, and $G_{cli}(s)$ is closed-loop transfer function of the current loop.

If virtual impedance is not introduced, the equivalent output impedance $Z_{ov}(s)$ is equal to $Z_o(s)$. As illustrated in [36], the stability margin is enhanced with a reduced inverter output impedance. Meanwhile, the dynamic performance is improved since the dominant eigenvalues moves from right to left. However, with small output impedance, the in-rush current can't be effectively mitigated during start-up or when plugging in different DG units [40]. Moreover, the harmonic performance and voltage unbalance compensation are also influenced by the inverter output impedance [36].

The MIOII scheme can be classified into the output current feedforward control strategy [37] and the inverter current feedforward control strategy [36]. The evaluation and comparison of these two methods are given in this subsection.

1) Output Current Feedforward Control (OCFC): When the

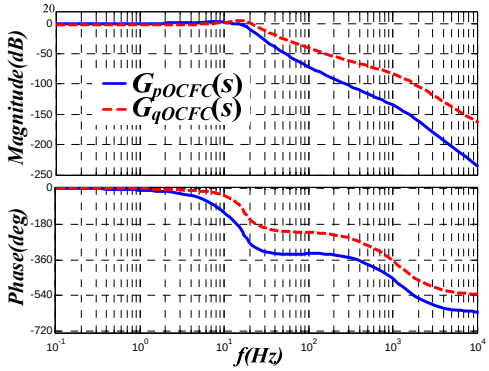

(a)

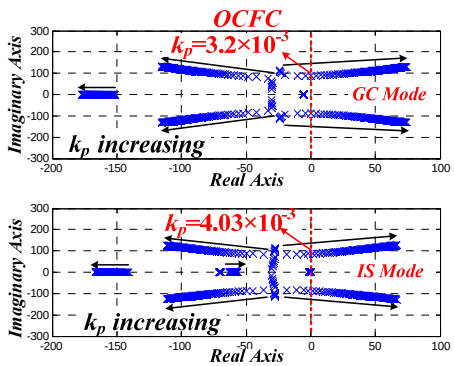

(b)

Fig. 13. OCFC scheme. (a) Closed-loop characteristics of droop loops in GC mode. (b). Root locus of low-frequency dominant eigenvalues for $0.785\times10^{-3}\leq k_p\leq31.4\times10^{-3}$ in different operation modes.

OCFC scheme presented in Fig. 12 is adopted, the equivalent output impedance can be obtained as (15):

$$\boldsymbol{Z_{ov}(s)} = \begin{bmatrix} (1-k_{cg}\cdot G_{cli}(s))Z_o(s) + Z_{v0}(s) & -G_{clu}(s)(\omega L_{v0}) \\ G_{clu}(s)(\omega L_{v0}) & (1-k_{cg}\cdot G_{cli}(s))Z_o(s) + Z_v(s) \end{bmatrix}$$
$$Z_{v0}(s) = G_{clu}(s)(R_{v0} + sL_{v0}) \tag{15}$$

where R_{v0} and L_{v0} are the initial virtual resistance and inductance, and k_{cg} is the feedforward gain which is set to 0.7 in this paper. The detailed design method of the feedforward gain k_{cg} can refer to [36] since the OCFC scheme is basically equivalent to the inverter current feedforward control strategy as verified with the analysis and experiment results below.

As shown in Fig. 13, the resonance peak can be suppressed and the stability margin can be enhanced with the OCFC scheme. Moreover, the control bandwidth is guaranteed and the dynamic performance can be improved. However, the promotion of stability margin mainly depends on the feedforward gain k_{cg}. Since the previously listed performance listed before may be influenced by the inverter output

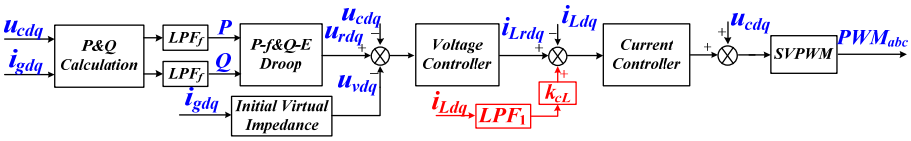

Fig. 14. Block diagram of the ICFC scheme.

impedance, the design of k_{cg} needs to be compromised.

2) Inverter Current Feedforward Control (ICFC): To avoid the current sensor requirement for i_{gabc} with the OCFC scheme, the ICFC scheme can be applied to realize the similar performance as OCFC scheme. As shown in Fig. 14, the inverter current i_{Ldq} with a low-pass filter LPF_1 substitutes for i_{gdq}. The feedforward gain k_{cL} is chosen to be the same as k_{cg}. Moreover, LPF_1 is a one-order LPF and the cut-off frequency is 1kHz. The detailed design process of the control parameters can be seen in [36].

As shown in Fig. 15(a), the closed-loop characteristics of the ICFC scheme basically coincide with the OCFC scheme as displayed in Fig. 13(a). Therefore, the control bandwidth and dynamic performance are equivalent to the OCFC scheme. Nevertheless, the stability margin of the ICFC scheme is slightly worse than the OCFC scheme in both operation modes as shown in Fig. 15(b). Moreover, the LPF_1, which is used to eliminate the current ripple of i_{Ldq}, also has an important impact on stability [36].

V. Experimental Validation

In order to verify the correctness of the above analysis, experiments based on a 2kVA prototype as shown in Fig. 16 are implemented. The controller is realized in the RT-LAB environment. The power stage parameters and control parameters of the prototype are listed in Table I and Table II, respectively. As seen in the root locus of the different methods, the trend of low-frequency stability in IS mode is very similar to that in GC mode. Therefore, it is concentrated on GC mode in this subsection to avoid unnecessary details. The experimental results are given as follows. In order to avoid triggering overcurrent protection which can be induced by the overshoot when P_0 steps or the low-frequency oscillation when k_p steps in GC mode, the step of P_0 and the value of P_0 when k_p steps are both set as 500W in the experimental validation.

A. Conventional Control Strategy

The low-frequency dominant eigenvalues with the conventional droop control strategy can be obtained through the small-signal model adopted in this paper. The boundary values of k_p with the conventional control strategy are 1.095×10^{-3} in GC mode and 1.280×10^{-3} in IS mode as shown in Fig. 4. Note that the boundary value is the value in which the system is under the critical stable state. Moreover, it can be illustrated from Fig. 17(b) and Fig. 17(c) that the practical

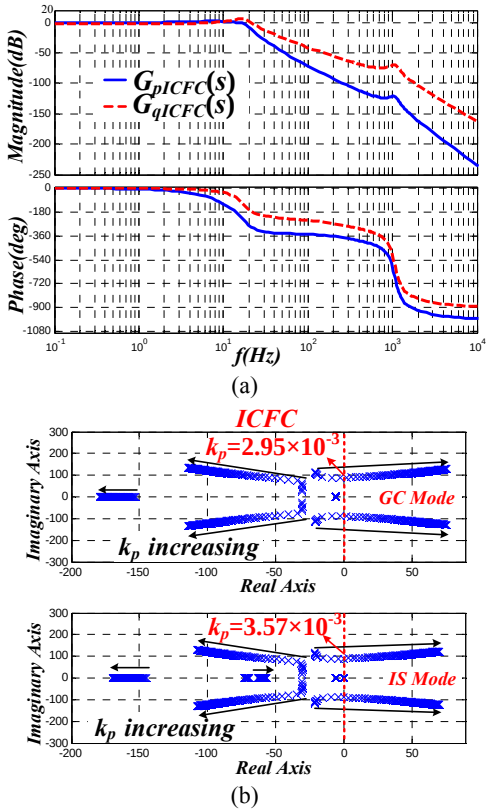

Fig. 15. ICFC scheme. (a) Closed-loop characteristics of droop loops in GC mode. (b) Root locus of low-frequency dominant eigenvalues for $0.785\times10^{-3}\leq k_p\leq31.4\times10^{-3}$ in different operation modes.

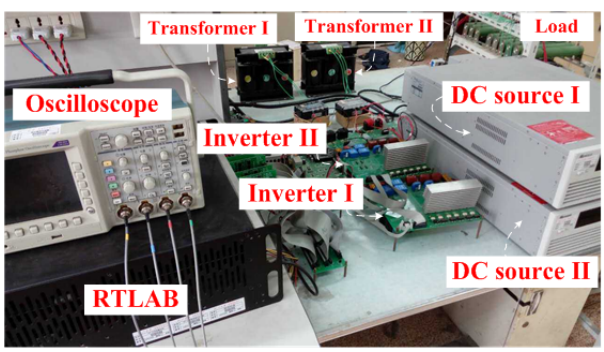

Fig. 16. Picture of the experimental prototype.

boundary values in the experiments are 1.1×10^{-3} in GC mode and 1.34×10^{-3} in IS mode. Comparing the modeling results with the experimental results, it can be concluded that the theoretical analysis of the adopted small-signal model in this paper basically coincides with the experimental results.

In GC mode, the transient process is activated by stepping

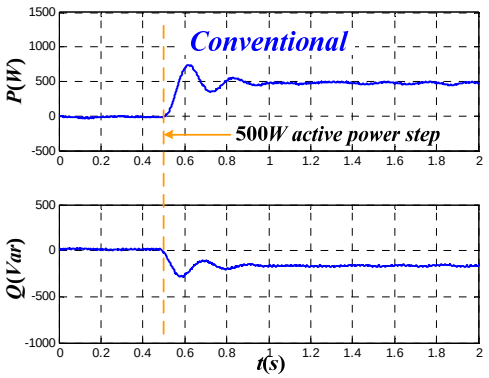

(a)

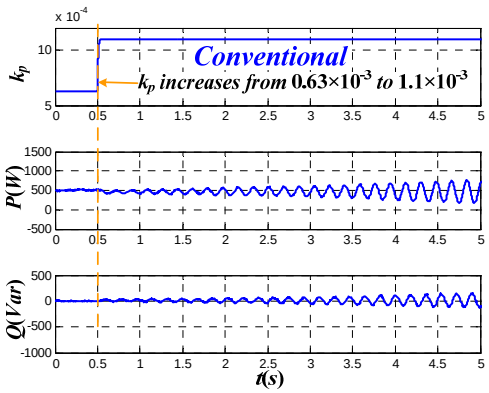

(b)

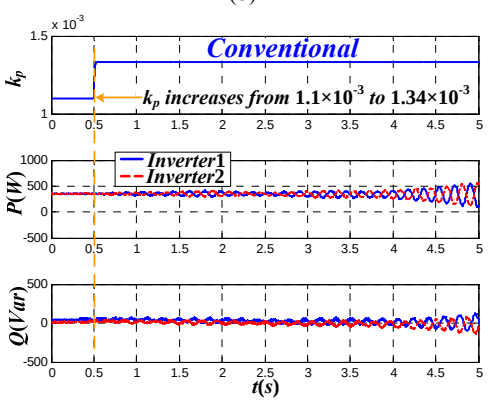

(c)

Fig. 17. Experimental results of active power P and reactive power Q with the conventional strategy in GC mode, respectively: (a)P_0 steps from 0 to 500W when k_p=0.63×10-3, (b)k_p increases from 0.63×10^{-3} to 1.1×10^{-3} with P_0=500W. (c)k_p increases from 1.1×10^{-3} to 1.34×10^{-3} with 800W load in IS mode.

the power instruction P_0. As shown in Fig. 17(a), stability is guaranteed in both GC mode and IS mode with a small k_p, which is lower than the rated value. Moreover, low-frequency oscillation is activated with a k_p step as presented in Fig. 17(b). Therefore, stable operation can't be satisfied with the rated value of k_p, and stability margin is very limited with the conventional control strategy.

B. The Source-type Damping Strategies

As seen in Fig. 18(a), the low-frequency oscillation is mitigated with the APFC scheme. Note that in case of

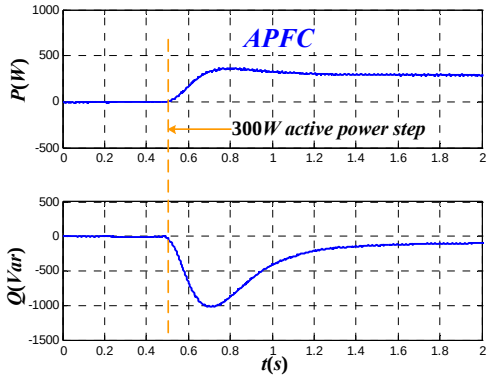

(a)

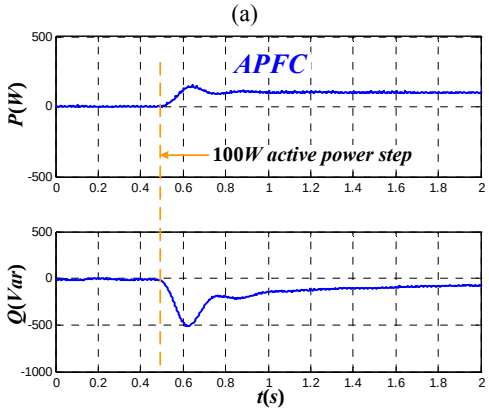

(b)

Fig. 18. APFC strategy in GC mode: (a)P_0 steps from 0 to 300W when k_p=1.57×10^{-3}, (b)P_0 steps from 0 to 100W when k_p=4.71×10^{-3}.

triggering the over-current protection for the coupling between the active power and the reactive power, the power step instruction is reduced in the experiment. Moreover, the stability margin is also significantly enhanced since stability is still ensured with a k_p that is three times larger than the rated value as presented in Fig. 18(b). Nevertheless, a large overshoot occurs in the reactive power when a small active power step is implemented. Meanwhile, the overshoot increases with a larger k_p. Hence, the coupling between the active power and the reactive power is obviously strengthened with the APFC scheme.

As shown in Fig. 19(a)-(b), stability is enhanced with the PD-CNIC scheme while the promotion of stability margin is much lower than the APFC scheme due to the lack of enough control degree of freedom. In addition, the low-frequency noise which can trigger the overcurrent protection is also introduced in IS mode as seen in Fig. 19(c)-(d). Since the isolation transformer is not ideal in the experiment, the voltage control is easy to be degraded in IS mode. However, in GC mode, voltage is mainly clamped by the stiff grid and the impact of a non-ideal isolation transformer can be mitigated. Consequently, the low-frequency noise is more serious in IS mode.

Since the degree of freedom is larger than that in the PD-CNIC scheme, the adjustment range turns to be wider with the proposed LL-CNIC scheme. As presented in Fig.

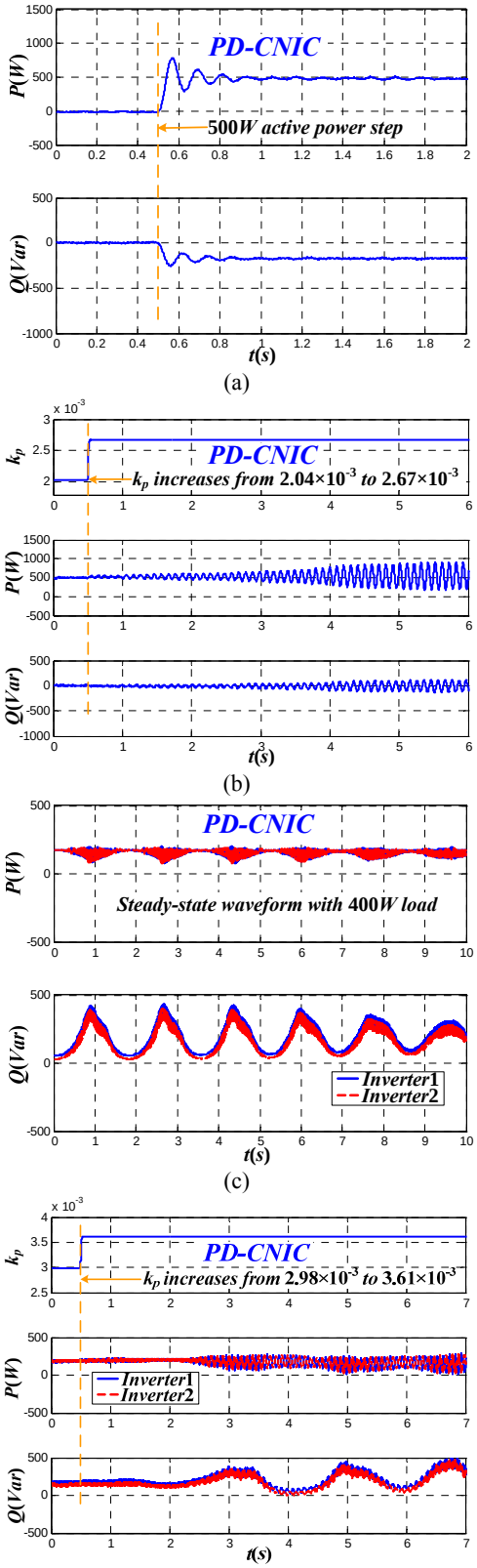

Fig. 19. PD-CNIC strategy. (a) P_0 steps from 0 to 500W when k_p=1.57×10^{-3} in GC mode, (b) k_p increases from 2.04×10^{-3} to 2.67×10^{-3} with P_0=500W in GC mode. (c) Steady-state waveforms when k_p=1.57×10^{-3} with 400W load in IS mode. (d) k_p increases from 2.98×10^{-3} to 3.61×10^{-3} with 400W load in IS mode.

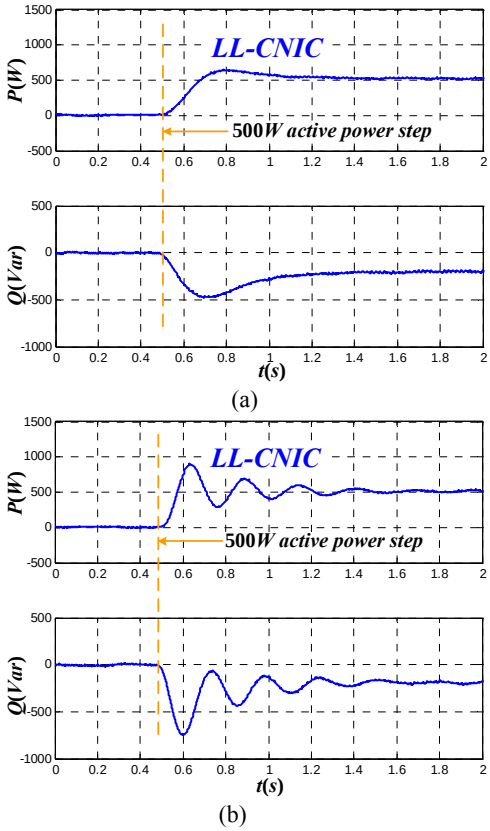

Fig. 20 Proposed LL-CNIC strategy in GC mode: P_0 steps from 0 to 500W when (a)k_p=1.57×10^{-3}, (b)k_p=4.71×10^{-3}.

20(a), stability can be guaranteed with the LL-CNIC scheme at the rated value of k_p. Moreover, when k_p is three times larger, stability is still ensured as displayed in Fig. 20(b). Therefore, stability can be effectively enhanced with the LL-CNIC scheme, and it is a very good choice when attempting to improve stability.

C. The Impedance-type Damping Strategies

As shown in Fig. 21(a), the low-frequency oscillation is effectively mitigated and stability is ensured with the VIC scheme at the rated value of k_p. Moreover, stability is still guaranteed with a k_p that is four times larger as presented in Fig. 21(b). In addition, the VIC scheme is immune to high-frequency noise when neglecting the derivative terms in practical applications.

Compared with the conventional control strategy, stability is guaranteed at the rated value of k_p with the OCFC scheme as presented in Fig. 22(a) although low-frequency damped oscillation exists. Nevertheless, since low-frequency oscillation occurs with a slightly higher k_p than the rated value as shown in Fig. 22(b), stability margin is still limited because of the restraint of feedforward gain k_{cg}.

With the ICFC scheme, stability is ensured with the rated k_p as displayed in Fig. 23(a) in spite of the damped oscillation. Nevertheless, stability margin is still limited as in the OCFC scheme as presented in Fig. 23(b). Hence, the ICFC scheme is basically equivalent to the OCFC scheme when ignoring

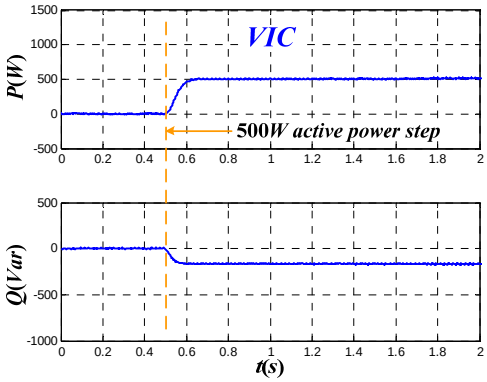

(a)

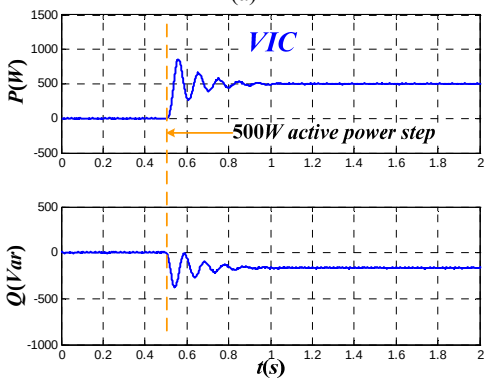

(b)

Fig. 21. VIC strategy in GC mode: P_0 steps from 0 to 500W when (a)k_p=1.57×10^{-3}, (b)k_p=6.28×10^{-3}.

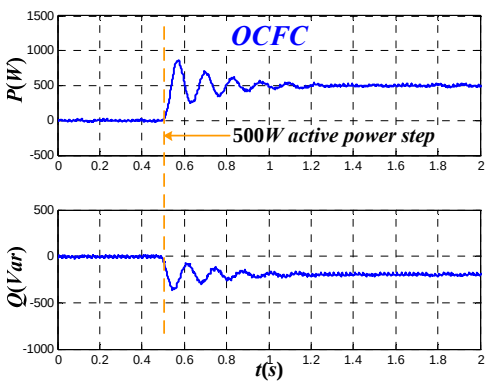

(a)

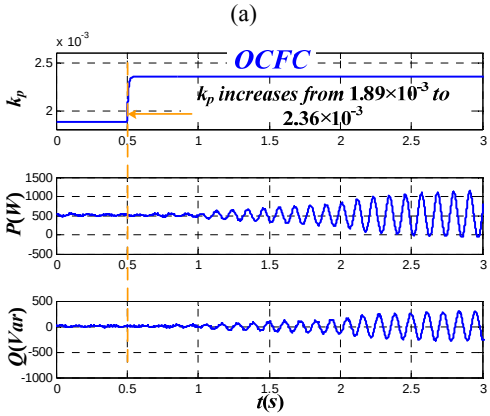

(b)

Fig. 22. OCFC strategy in GC mode. (a) P_0 steps from 0 to 500W when k_p=1.57×10^{-3}. (b) k_p increases from 1.89×10^{-3} to 2.36×10^{-3} with P_0=500W.

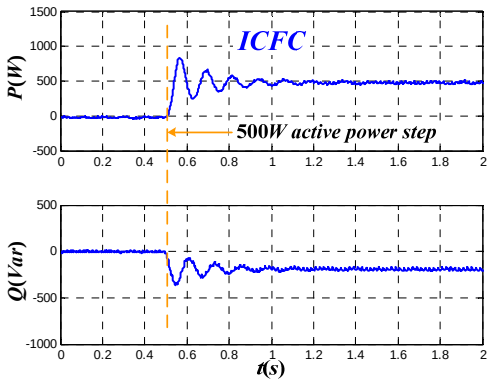

(a)

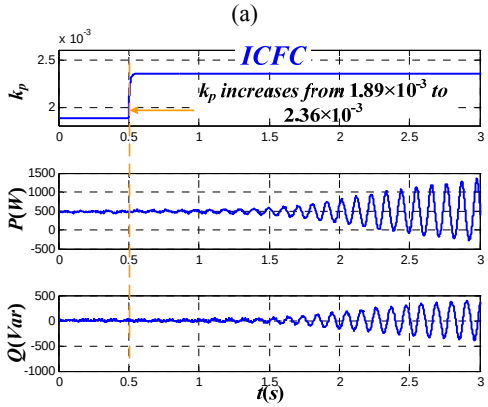

(b)

Fig. 23. ICFC strategy in GC mode. (a) P_0 steps from 0 to 500W with k_p=1.57×10^{-3}. (b) k_p increases from 1.89×10^{-3} to 2.36×10^{-3} with P_0=500W.

this minor difference.

VI. Comparison and Discussion

Different damping strategies have been evaluated and analyzed in section III and section IV. The comparison and synthesis of different damping methods are discussed below.

A. Comparison between Different Damping Methods

Although the low-frequency stability can be improved with both types of damping methods, the individual impacts on the system performance are different.

The comparison between the source-type damping methods and the impedance-type damping methods is shown in Fig. 24(a). As can be seen, the source-type damping methods may introduce side-effects in the low-frequency range, such as power coupling and low-frequency noise. Moreover, the performance relies heavily on the structure and parameters of the compensation networks. The high frequency performance, such as harmonic performance, voltage unbalance performance and transient current-limiting performance, is influenced by the impedance-type damping methods because the impedance characteristics are changed. Therefore, the source-type damping methods should be applied in fields where high frequency performance is not expected to be changed. However, the impedance-type damping methods

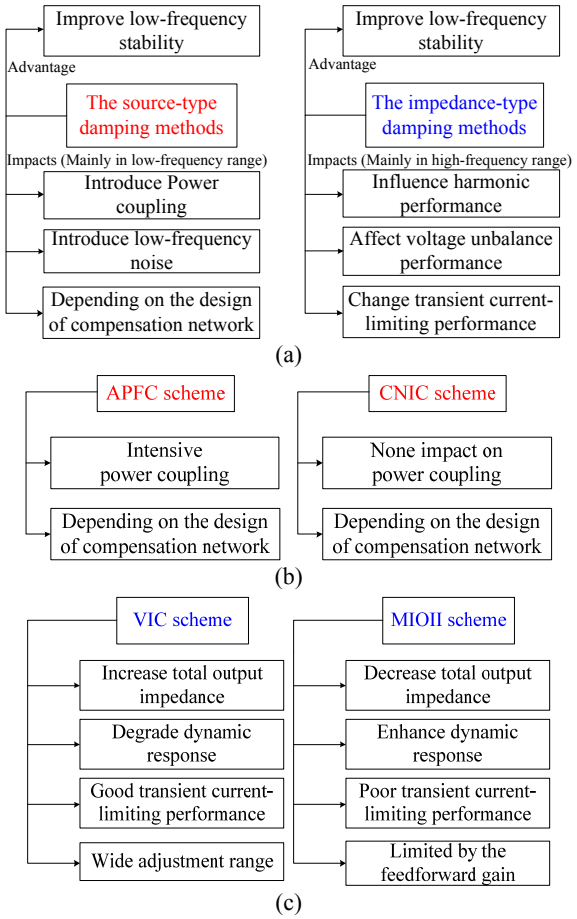

Fig. 24. (a) Comparison between different types of damping methods. (b) Comparison between APFC scheme and CNIC scheme. (c) Comparison between VIC scheme and the MIOII scheme.

can be applied in fields where the high frequency performance is compatible and low-frequency side-effects are intolerable.

In addition to the function of enhancing the low-frequency stability, the impacts of the source-type damping methods and the impedance-type damping methods are different. Therefore, the comparison between the constituent parts of each method is implemented as follows:

1) Since the source-type damping strategies consist of the APFC scheme and the CNIC scheme, the comparison between these schemes is shown in Fig. 24(b). As shown, intensive power coupling is introduced by the APFC scheme while the CNIC scheme has no impact on the power coupling. In addition, both schemes are significantly influenced by the structure and parameters of the compensation networks. Meanwhile, the adjustment range of both schemes is often determined by the control degrees of freedom of the compensation network. Therefore, with properly designed compensation networks, the CNIC scheme may be a good choice.

2) The impedance-type damping methods include the VIC scheme and the MIOII scheme. Since the output impedance is

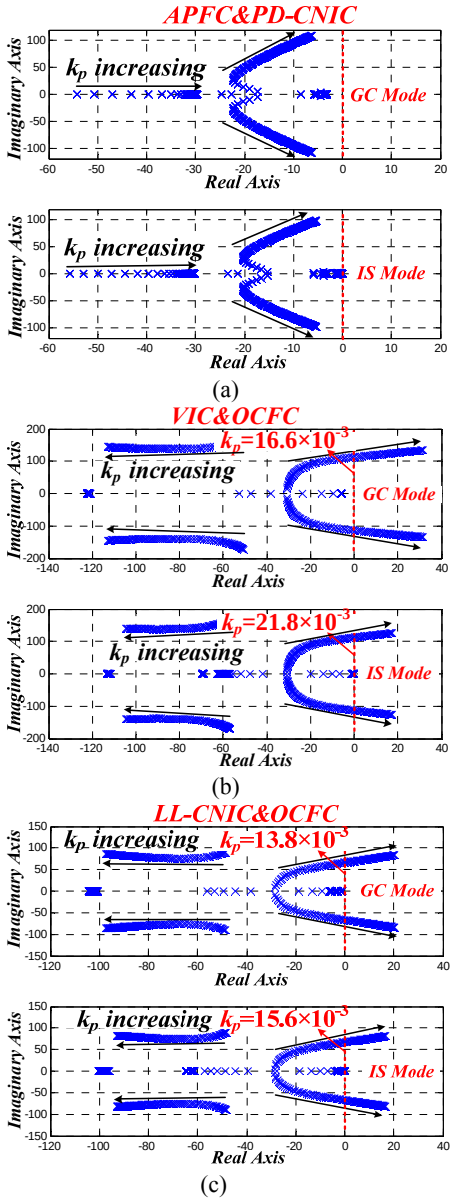

Fig. 25. Root locus of low-frequency dominant eigenvalues for $0.785\times10^{-3}\leq k_p\leq31.4\times10^{-3}$ in different operation modes: (a) with the synthesis of APFC scheme and PD-CNIC scheme, (b) with the synthesis of VIC scheme and OCFC scheme and (c) with the synthesis of LL-CNIC scheme and OCFC scheme.

increased by the VIC scheme and reduced by the MIOII scheme, the characteristics of the VIC scheme are basically contrary to the MIOII scheme as shown in Fig. 24(c). In addition, the adjustment range of the MIOII scheme is limited by the feedforward gain since the stability might be degraded by negative impedance. However, a wide adjustment range can be guaranteed by changing the virtual impedance with the VIC scheme. Therefore, the VIC scheme can be applied in fields demanding a high output impedance, while the MIOII scheme should be applied in low output impedance fields.

Consequently, different damping methods have different advantages and disadvantages. Fortunately, there are no conflicts among different damping strategies. Therefore,

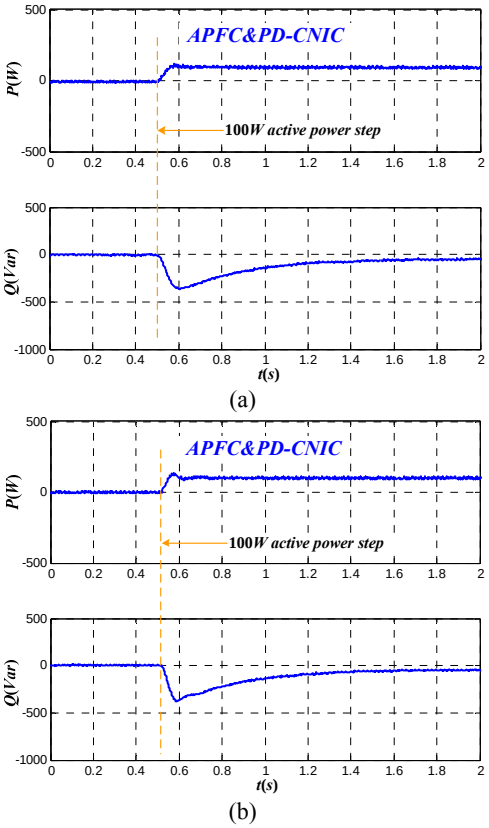

Fig. 26. Experimental results of the synthesis of APFC scheme and PD-CNIC scheme when P_0 steps from 0 to 500W in GC mode with: (a) k_p=4.71×10^{-3} and (b) k_p=8.32×10^{-3}.

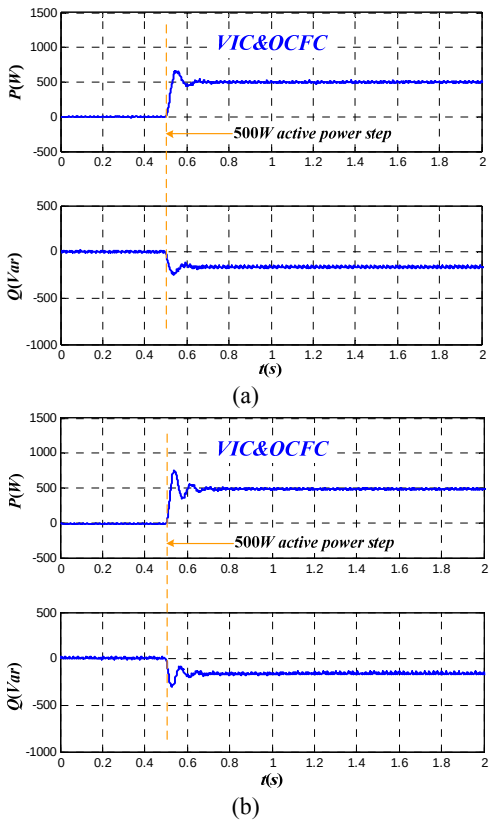

Fig. 27. Experimental results of the synthesis of VIC scheme and OCFC scheme when P_0 steps from 0 to 500W in GC mode with: (a) k_p=6.28×10^{-3} and (b) k_p=10.36×10^{-3}.

these damping strategies can also be combined to enhance stability.

B. Synthesis of Different Damping Methods

Three types of combinations between different damping methods can be achieved: the synthesis of source-type damping strategies, the synthesis of impedance-type strategies and the synthesis of the source-type damping strategy and the impedance-type damping strategy. To better illustrate the effect of these combinations on stability, one possible combination for each type is given and analyzed in this subsection.

For the source-type damping strategies, the APFC scheme and the CNIC scheme can be combined to improve stability. For example, the root locus of low-frequency dominant eigenvalues with the synthesis of the APFC scheme and the PD-CNIC scheme is presented in Fig. 25(a). Compared with Fig. 6(b) and Fig. 8(b), the stability margin is significantly enhanced. Moreover, the low-frequency noise introduced by the PD-CNIC scheme can be suppressed with the feedforward of active power in the APFC scheme. However, the effect of the coupling between active power and reactive power introduced by the APFC scheme can't be avoided.

For impedance-type damping strategies, stability is also enhanced through synthesizing the VIC strategy and the MIOII strategy as shown in Fig. 25(b). Compared with Fig. 11(b) and Fig. 13(b), the stability is further strengthened. However, output impedance is often changed by the impedance-type damping strategies. Moreover, harmonic performance, voltage unbalance and dynamic response are significantly influenced by the output impedance [36], [38]-[39]. Consequently, the controller design in the case of synthesis should comprehensively weigh the impacts on stability and high-frequency performance.

In addition, the synthesis of the source-type damping strategy and the impedance-type damping strategy is also very helpful in the promotion of stability margin. As displayed in Fig. 25(c), the stability margin is significantly enhanced through the combination between LL-CNIC scheme and the OCFC scheme.

Based on the above analysis, it can be concluded that stability can be further enhanced with the synthesis of different damping methods. Nevertheless, the disadvantages of each method may be introduced through the synthesis. Therefore, trade-off and comprehensive evaluation are needed when considering the synthesis of different damping methods.

C. Experimental Validation

In order to verify the theoretical analysis for the synthesis of different damping methods, experimental validation is presented in this subsection.

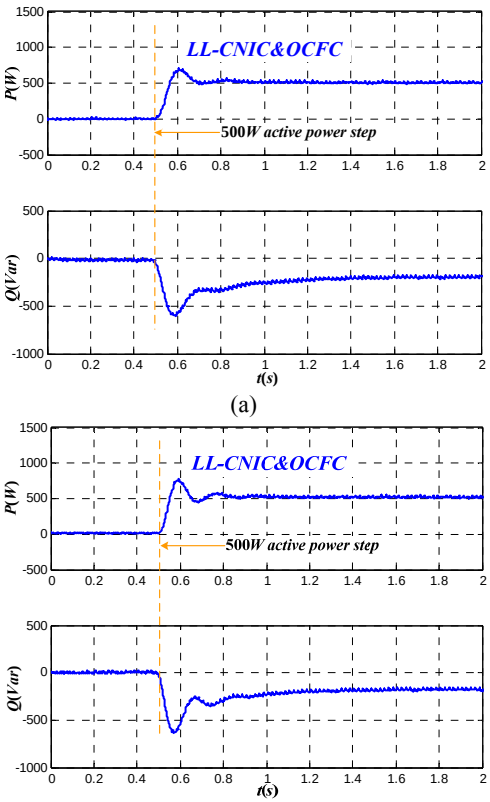

Fig. 28. Experimental results of the synthesis of LL-CNIC scheme and OCFC scheme when P_0 steps from 0 to 500W in GC mode with: (a) k_p=4.71×10^{-3} and (b) k_p=6.28×10^{-3}.

As shown in Fig. 26(b), when k_p=8.32×10^{-3}, which is larger than the boundary value of the APFC scheme and the PD-CNIC scheme, stability is still guaranteed. However, the coupling of active power and reactive power introduced by the APFC scheme also exists. In addition, comparing Fig. 26(a) with Fig. 18(b), better low-frequency damping and smaller overshoot of reactive power also signify the reinforce of stability through the synthesis of the APFC scheme and the PD-CNIC scheme.

Comparing Fig. 27(a) with Fig. 21(b), low-frequency oscillation in the same value of k_p is better mitigated with the combination of the VIC scheme and the OCFC scheme. Meanwhile, as presented in Fig. 27(b), stability is ensured when k_p=10.36×10^{-3}, which is larger than the boundary value of the VIC scheme as shown in Fig. 11(b).

Better low-frequency damping presents in Fig. 28(a) through the comparison with Fig. 20(b). Moreover, as shown in Fig. 28(b), stability is guaranteed with a larger value of k_p than the boundary value of the LL-CNIC scheme. Therefore, better low-frequency damping performance is achieved through the synthesis of the LL-CNIC scheme and the OCFC scheme.

VII. Conclusion

In this paper, low-frequency oscillation issues are analyzed for the conventional droop control strategy and the oscillation damping strategies are classified into two categories: the source-type damping strategy and the impedance-type damping strategy. The source-type damping strategy consists of the APFC scheme and the CNIC scheme, while the impedance-type damping strategy includes the VIC scheme and the MIOII scheme. The advantages and disadvantages of each damping strategy are theoretically evaluated and experimentally validated. Moreover, comparison among different methods is implemented to illustrate the suitable application fields of each method. Finally, the synthesis of different damping methods is discussed to significantly improve the low-frequency stability, and experiment results verify the stability improvement.

Acknowledgment

This work is sponsored by the National High-Tech R&D Program of China (2011AA050202).

References

[1] F. Blaabjerg, R. Teodorescu, M. Liserre, and A. V. Timbus, "Overview of control and grid synchronization for distributed power generation systems," *IEEE Trans. Ind. Electron.*, Vol. 53, No. 5, pp. 1398-1409, Oct. 2006.

[2] R. H. Lasseter, "MicroGrids," in *Proc. IEEE Power Eng. Soc. Winter Meet.*, 2002, pp. 305-308.

[3] Z. Li, C. Zang, P. Zeng, H. Yu, H. Li, and S. Li, "Analysis of multi-agent-based adaptive droop-controlled AC microgrids with PSCAD: modeling and simulation", *Journal of Power Electronics*, Vol. 15, No. 2, pp.455-468, Mar. 2015.

[4] J. M. Guerrero, M. Chandorkar, T. Lee, and P. C. Loh, "Advanced control architectures for intelligent microgrids-part I: Decentralized and hierarchical control," *IEEE Trans. Ind. Electron.*, Vol. 60, No. 4, pp. 1254-1262, Apr. 2013.

[5] J. Rocabert, A. Luna, F. Blaabjerg, and P. Rodriguez, "Control of power converters in AC microgrids," *IEEE Trans. Power Electron.*, Vol. 27, No. 11, pp. 4734-4749, Nov. 2012.

[6] Q.-C. Zhong, "Robust droop controller for accurate proportional load sharing among inverters operated in parallel," *IEEE Trans. Ind. Electron.*, Vol. 60, No. 4, pp. 1281-1290, Apr. 2013.

[7] J. C. Vasquez, J. M. Guerrero, M. Savaghebi, J. Eloy-Garcia, and R. Teodorescu, "Modeling, analysis, and design of stationary-reference-frame droop-controlled parallel three-phase voltage source inverters," *IEEE Trans. Ind. Electron.*, Vol. 60, No. 4, pp. 1271-1280, Apr. 2013.

[8] Q. Zhang, Y. Liu, C. Wang, and N. Wang, "Parallel operation of microgrid inverters based on adaptive sliding-mode and wireless load-sharing controls," *Journal of Power Electronics*, Vol. 15, No. 3, pp.741-752, May 2015.

[9] X. Wang, F. Blaabjerg, and W. Wu, "Modeling and analysis of harmonic stability in an AC power-electronics-based power system," *IEEE Trans. Power Electron.*, Vol. 29, No. 12, pp. 6421-6432, Dec. 2014.

[10] R. Majumder, "Some aspects of stability in microgrids," *IEEE Trans. Power Syst.*, Vol. 28, No. 3, pp. 3243-3252,

Aug. 2013.
[11] N. Pogaku, M. Prodanovic, and T. C. Green, "Modeling, analysis and testing of autonomous operation of an inverter-based microgrid," *IEEE Trans. Power Electron.*, Vol. 22, No. 2, pp. 613-625, Mar. 2007.
[12] E. Barklund, N. Pogaku, M. Prodanovic, C. Hernandez-Aramburo, and T. C. Green, "Energy management in autonomous microgrid using stability-constrained droop control of inverters," *IEEE Trans. Power Electron.*, Vol. 23, No. 5, pp. 2346-2352, Sep. 2008.
[13] J. He and Y. W. Li, "Analysis, design, and implementation of virtual impedance for power electronics interfaced distributed generation," *IEEE Trans. Ind. Appl.*, Vol. 47, No. 6, pp. 2525-2538, Nov./Dec. 2011.
[14] J. He and Y. W. Li, "Generalized Closed-Loop control schemes with embedded virtual impedances for voltage source converters with LC or LCL filters," *IEEE Trans. Power Electron.*, Vol. 27, No. 4, pp. 1850-1861, Apr. 2012.
[15] X. Wang, Y. W. Li, F. Blaabjerg, and P. C. Loh, "Virtual-impedance-based control for voltage-source and current-source converters," *IEEE Trans. Power Electron.*, Vol. 30, No. 12, pp. 7019-7037, Dec. 2015.
[16] A. Kahrobaeian and Y. A. R. Mohamed, "Analysis and mitigation of low-frequency instabilities in autonomous medium-voltage converter-based microgrids with dynamic loads," *IEEE Trans. Ind. Electron.*, Vol. 61, No. 4, pp. 1643-1658, Apr. 2014.
[17] N. Bottrell, M. Prodanovic, and T. C. Green, "Dynamic stability of a microgrid with an active load," *IEEE Trans. Power Electron.*, Vol. 28, No. 11, pp. 5107-5119, Nov. 2013.
[18] A. A. A. Radwan and Y. A. R. I. Mohamed, "Modeling, analysis, and stabilization of converter-fed AC microgrids with high penetration of converter-interfaced loads," *IEEE Trans. Smart Grid*, Vol. 3, No. 3, pp. 1213-1225, Sep. 2012.
[19] C. Wan, M. Huang, C. K. Tse, and X. Ruan, "Effects of interaction of power converters coupled via power grid: a design-oriented study," *IEEE Trans. Power Electron.*, Vol. 30, No. 7, pp. 3589-3600, Jul. 2015.
[20] Z. Liu, J. Liu, W. Bao, and Y. Zhao, "Infinity-norm of impedance based stability criterion for three-phase AC distributed power systems with constant power loads," *IEEE Trans. Power Electron.*, Vol. 30, No. 6, pp. 3030-3043, Jun. 2015.
[21] C. Wan, M. Huang, C. K. Tse, S. Wong, and X. Ruan, "Nonlinear behavior and instability in a three-phase boost rectifier connected to a nonideal power grid with an interacting load," *IEEE Trans. Power Electron.*, Vol. 28, No. 7, pp. 3255-3265, Jul. 2013.
[22] J. M. Guerrero, J. Matas, L. Garcia De Vicuna, M. Castilla, and J. Miret, "Wireless-Control strategy for parallel operation of distributed-generation inverters," *IEEE Trans. Ind. Electron.*, Vol. 53, No. 5, pp. 1461-1470, Jan. 2006.
[23] J. C. Vasquez, J. M. Guerrero, A. Luna, P. Rodríguez, and R. Teodorescu, "Adaptive droop control applied to voltage-source inverters operating in grid-connected and islanded modes," *IEEE Trans. Ind. Electron.*, Vol. 56, No. 10, pp. 4088-4096, Oct. 2009.
[24] J. M. Guerrero, L. G. de Vicuna, J. Matas, M. Castilla, and J. Miret, "A wireless controller to enhance dynamic performance of parallel inverters in distributed generation systems," *IEEE Trans. Power Electron.*, Vol. 19, No. 5, pp. 1205-1213, Sep. 2004.
[25] N. H. Kan'An, P. Kanjiya, H. H. Zeineldin, W. Xiao, J. L. Kirtley, and V. Khadkikar, "A modified control topology to improve stability margins in micro-grids with droop controlled IBDG," in *Proc. Renew. Power Gener. Conf.*, pp. 1-7, 2014.
[26] C. T. Lee, C. C. Chu, and P. T. Cheng, "A new droop control method for the autonomous operation of distributed energy resource interface converters," *IEEE Trans. Power Electron.*, Vol. 28, No. 4, pp. 1980-1993, Apr. 2013.
[27] Y. A. R. I. Mohamed and E. F. El-Saadany, "Adaptive decentralized droop controller to preserve power sharing stability of paralleled inverters in distributed generation microgrids," *IEEE Trans. Power Electron.*, Vol. 23, No. 6, pp. 2806-2816, Nov. 2008.
[28] M. B. Delghavi and A. Yazdani, "An adaptive feedforward compensation for stability enhancement in droop-controlled inverter-based microgrids," *IEEE Trans. Power Del.*, Vol. 26, No. 3, pp. 1764-1773, Jul. 2011.
[29] R. Majumder, B. Chaudhuri, A. Ghosh, R. Majumder, G. Ledwich, and F. Zare, "Improvement of stability and load sharing in an autonomous microgrid using supplementary droop control loop," *IEEE Trans. Power Syst.*, Vol. 25, No. 2, pp. 796-808, May 2010.
[30] E. Z. Zhou, O. P. Malik, and G. S. Hope, "Design of stabilizer for a multimachine power system based on the sensitivity of PSS effect," *IEEE Trans. Energy Convers.*, Vol. 7, No. 3, pp. 606-613, Sep. 1992.
[31] C. Y. Chung, K. W. Wang, C. T. Tse, and R. Niu, "Power-system stabilizer (PSS) design by probabilistic sensitivity indexes (PSIs)," *IEEE Trans. Power Syst.*, Vol. 17, No. 3, pp. 688-693, Aug. 2002.
[32] P. Kundur, M. Klein, G. J. Rogers, and M. S. Zywno, "Application of power system stabilizers for enhancement of overall system stability," *IEEE Trans. Power Syst.*, Vol. 4, pp. 614-626, May 1989.
[33] P. Kundur, *Power system stability and control*, McGraw-Hill Professional, 1994.
[34] J. Liu, Y. Miura, and T. Ise, "Comparison of dynamic characteristics between virtual synchronous generator and droop control in Inverter-Based distributed generators," in *Proc. Inter. Power Electron. Conf.*, pp. 1536-1543, 2014.
[35] T. Shintai, Y. Miura, and T. Ise, "Oscillation damping of a distributed generator using a virtual synchronous generator," *IEEE Trans. Power Del.*, Vol. 29, No. 2, pp. 668-676, Apr. 2014.
[36] Y. Tao, Q. Liu, Y. Deng, X. Liu, and X. He, "Analysis and mitigation of inverter output impedance impacts for distributed energy resource interface," *IEEE Trans. Power Electron.*, Vol. 30, No. 7, pp. 3563-3576, Jul. 2015.
[37] Z. Liu, J. Liu, and Y. Zhao, "A unified control strategy for three-phase inverter in distributed generation," *IEEE Trans. Power Electron.*, Vol. 29, No. 3, pp. 1176-1191, Mar. 2014.
[38] Q. Liu, Y. Tao, X. Liu, Y. Deng, and X. He, "Voltage unbalance and harmonics compensation for islanded microgrid inverters," *IET Power Electron.*, Vol. 7, No. 5, pp. 1055-1063, May 2014.
[39] X. Wang, F. Blaabjerg, and Z. Chen, "Autonomous control of inverter-interfaced distributed generation units for harmonic current filtering and resonance damping in an islanded microgrid," *IEEE Trans. Ind. Appl.*, Vol. 50, No. 1, pp. 452-461, Jan./Feb. 2014.
[40] J. M. Guerrero, J. C. Vasquez, J. Matas, M. Castilla, and L. G. de Vicuna, "Control strategy for flexible microgrid based on parallel line-interactive UPS systems," *IEEE Trans. Ind. Electron.*, Vol. 56, No. 3, pp. 726-736, Mar. 2009.

Yong Tao received the B.Sc. degree in Electrical Engineering from Nanjing University of Science and Technology, Nanjing, China, in 2011, where he is currently working toward the Ph.D degree from the College of Electrical Engineering, Zhejiang University, Hangzhou, China. His research interests include microgrid control, distributed generation and energy management.

Yan Deng received the B.E.E. degree from the Department of Electrical Engineering, Zhejiang University, Hangzhou, China, in 1994, and the Ph.D. degree in power electronics and electric drives from the College of Electrical Engineering, Zhejiang University, in 2000. Since 2000, he has been a faculty member at Zhejiang University, teaching and conducting research on power electronics. He is currently an Associate Professor. His research interests are topologies and control for switch-mode power conversion.

Guangdi Li received the B.Sc. degree in Electrical Engineering from Northeastern University, Shenyang, China, in 2013. He is currently working toward the M.Sc degree from the College of Electrical Engineering, Zhejiang University, Hangzhou, China. His research interests include AC microgrid, energy storage system, three-phase inverters and their control methods.

Guipeng Chen received the B.E.E. degree from the Department of Electrical Engineering, Zhejiang University, Hangzhou, China, in 2011. He is currently working toward the Ph.D degree from the College of Electrical Engineering, Zhejiang University, Hangzhou, China. His current research interests include soft-switching DC-DC converters, bi-directional DC-DC converters and multi-port DC-DC converters.

Xiangning He (M'95--SM'96--F'10) received the B.Sc. and M.Sc. degrees from Nanjing University of Aeronautical and Astronautical, Nanjing, China, in 1982 and 1985, respectively, and the Ph.D. degree from Zhejiang University, Hangzhou, China, in 1989. From 1985 to 1986, he was an Assistant Engineer at the 608 Institute of Aeronautical Industrial General Company, Zhuzhou, China. From 1989 to 1991, he was a Lecturer at Zhejiang University. In 1991, he obtained a Fellowship from the Royal Society of U.K., and conducted research in the Department of Computing and Electrical Engineering, Heriot-Watt University, Edinburgh, U.K., as a Post-Doctoral Research Fellow for two years. In 1994, he joined Zhejiang University as an Associate Professor. Since 1996, he has been a Full Professor in the College of Electrical Engineering, Zhejiang University. He was the Director of the Power Electronics Research Institute and the Head of the Department of Applied Electronics, and he is currently the Vice Dean of the College of Electrical Engineering, Zhejiang University. His research interests are power electronics and their industrial applications. He is the author or co-author of more than 280 papers and one book "Theory and Applications of Multi-level Converters". He holds 22 patents. Dr. He received the 1989 Excellent Ph.D. Graduate Award, the 1995 Elite Prize Excellence Award, the 1996 Outstanding Young Staff Member Award and 2006 Excellent Staff Award from Zhejiang University for his teaching and research contributions. He received seven Scientific and Technological Achievements Awards from Zhejiang Provincial Government and the State Educational Ministry of China in 1998, 2002, 2009 and 2011 respectively, and six Excellent Paper Awards. Dr. He is a Fellow of The Institute of Electrical and Electronics Engineers (IEEE) and has been appointed as IEEE Distinguished Lecturer by the IEEE Power Electronics Society in 2011. He is also a Fellow of the Institution of Engineering and Technology (formerly IEE), U.K.